Journal of Materials Chemistry C

Accepted Manuscript

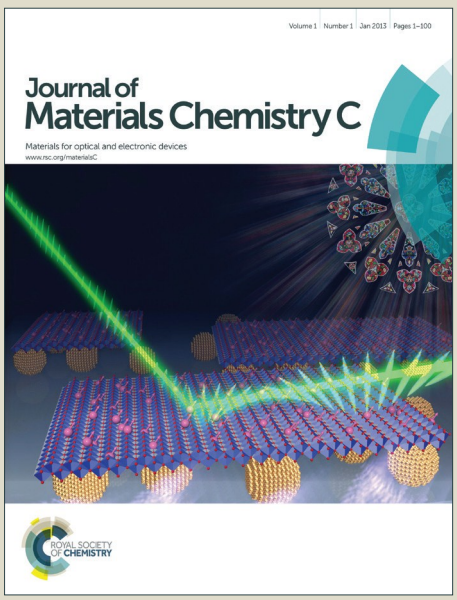

ROYAL SOCIETY OF CHEMISTRY

www.rsc.org/materialsC

Cite this: DOI: 10.1039/c0xx00000x

www.rsc.org/xxxxxx

ARTICLE TYPE

Manifestation of High Temperature Ferromagnetism in Fluorinated Graphite Carbon Nitride Nanosheets

Daqiang Gao, Yonggang Liu, Minyue Song, Shoupeng Shi, Mingsu Si*, Desheng Xue.

Received (in XXX, XXX) Xth XXXXXXXXX 20XX, Accepted Xth XXXXXXXXX 20XX

DOI: 10.1039/b000000x

Two-dimensional ferromagnetic metal-free materials possessing only an s/p electronic configuration with weak spin–orbit coupling and a large spin relaxation time, play a crucial role in constructing future spintronic devices. Here we demonstrate a novel two-dimensional material, fluorinated graphite carbon nitride (g-C_3N_4) nanosheets, do appear an intrinsic ferromagnetism, where its Curie temperature can reach as high as 700 K. More surprising is that such unusual ferromagnetism can be further tuned by changing the concentration of fluorine. This tuneable electronic spin-polarization as well as ferromagnetism observed in fluorinated g-C_3N_4 nanosheets is quite promising for future device applications in spintronics.

The miniaturization of silicon devices are now being reached as transistor gate lengths approach 5 nm owing to the limitation of Moore's law. Spintronics, which exploits the electron spin rather than the charge, will operate on a sub 1 nm length scale and thus facilitate another generation of devices, but depending on the ready availability of a material that is a semiconductor, as well as, is ferromagnetic at room temperature and has a highly tuneable band gap and magnetic coupling.[1,2] During the past years, efforts have been devoted to search for room temperature magnetic semiconductors in various host semiconductor materials by doping or defects engineering, to exploit their potential application in future spintronic devices.[3,4]

Recently, the magnetic properties of carbon-based materials ignited intense research interest because of their extreme importance in applications such as light metal-free magnets at room temperature.[5,6] Especially, metal-free ferromagnetic nanosheets with only s/p electronic structure present relatively weak spin–orbit coupling and could give a large spin relaxation time, which make this material very attractive for novel spintronic devices.[7,8] It is reported that ideal graphene is intrinsically nonmagnetic due to a delocalized π bonding network. However, some experimental results have confirmed that vacancies, adatoms, and zigzag edges can introduce localized magnetic moments by the formation of unpaired spins in graphene.[9,10] Unfortunately, the use of pristine graphene in electronics applications suffers from the drawback of zero band gap.[11]

Similar to the case of graphite, the graphitic carbon nitride (g-C_3N_4) lattices based on s-triazine and heptazine rings have two dimension (2D) π-conjugated planar layers because the triazine ring is aromatic.[12] However, the electronic structures of g-C_3N_4 differ significantly from those of graphite. In contrast to metallic graphite, g-C_3N_4 is semiconducting with a moderate band gap.[13] This makes the g-C_3N_4 function as a metal free polymeric photocatalyst for splitting water molecules with solar energy or its direct use in heterogeneous catalysis.[14-16] Further, the photoreactivity performance can be enhanced by doping g-C_3N_4 with sulfur or boron atoms, where dopant atoms play important roles in the electronic structure modification and the relevant applications.[17,18] Recently, with the rapid development of light nonmetallic magnets, studies have shown that the electron spin-polarization of these materials is closely related to vacancy defects.[19-21] The porous frameworks of g-C_3N_4 with well-ordered vacancies remind us of possible spin-polarization and even ferromagnetism of these materials. Unfortunately, g-C_3N_4 displays non-magnetic properties in its pristine form.[22,23] Very recently, Based on g-C_3N_4, some magnetic structures are predicted, such as kagome C_3N_4 sheet, 2D triangular graphene nanoflakes, as well as the half-metallicity magnetic material of g-C_4N_3.[24-26] However, although considerable efforts have been devoted in theoretically, the experimental synthesis of above expected C-N based materials is still a big challenge and it is urgent to develop effective methods.

Fluorination of carbon-based nanostructures is recently attracting a lot of interest as a methodology that allows for the tuning of their mechanical, electronic, and magnetic properties.[27-29] In contrast to direct manipulation of the carbon atoms, e.g., creating vacancies or reshaping edges, fluorination can effectively affect the electronic properties in a similar manner with the advantage of reversiblity process. For instance, fluorine atoms are introduced into graphene in the form of C-F covalent bond by XeF_2 fluorination.[30] Experimental and theoretical studies have indicated that the band gap of fluorinated graphene can be varied from 0 eV to about 3 eV with changing degrees of fluorination.[31] More

interestingly, magnetism can be induced in fluorinated graphene which is an ferromagnetic semiconductor.[32] Recently, Wang and coauthors revealed that fluorination not only provides a modified texture but also enables the effective adjustment of the electronic band gaps of g-C_3N_4 solid.[33] However, up to now, the electronic structures, and magnetic behaviors for the fluorinated g-C_3N_4 nanosheets are unclear, that is to say, it remains an open question whether fluorination could endow spin related information in g-C_3N_4 structure.

In this work, we report comprehensive experimental and first-principles studies on the electronic and magnetic properties of fluorinated g-C_3N_4 nanosheets. It is shown that the fluorinated g-C_3N_4 nanosheets exhibit high temperature ferromagnetism with the Curie temperature of 733 K. Interestingly, the room temperature saturation magnetization of the metal free nanosheets could even be tuned by changing the concentration of fluorine. Such stable electron spin-polarization and tuneable ferromagnetism are quite promising for the application of fluorinated g-C_3N_4 nanosheets in spintronics. At the same time, this work paves a new pathway to engineer the magnetic properties of 2D nanomaterial systems.

Results and discussions

The geometries, electronic and magnetic properties of fluorinated g-C_3N_4 monolayers are investigated through using first-principles calculations. To search for the most stable absorbed position of F atom, three configurations denoted as T_C (on the top site of C atom), T_N (on the top site of N atom), and T_{center} (above the center of the hexagonal ring) are considered. Compared to T_N and T_{center} (not shown for brevity), T_C is the most favourable, as shown in figure 1. Since there exist two non-equivalent C atoms in g-C_3N_4, two absorbed sites, i.e., T_{C1} and T_{C2} were taken into account in realistic calculations. Our calculations showed that the T_{C1} (Figure 1(a)) is more stable by around 0.1 eV than that of T_{C2} (Figure 1(b)). The bond lengths of F-C were estimated to be in the range of 1.43-1.44 Å. Owing to the formation of F-C bonds, partial C bonds were transformed from the sp^2 to the sp^3 hybridization. This transformation plays an important role in the formation of distortion, that is the C and N atoms no longer distribute at a planar plane (see the bottom panels of figure 1), as well as the introduction of unusual intrinsic ferromagnetism (discussed as below).

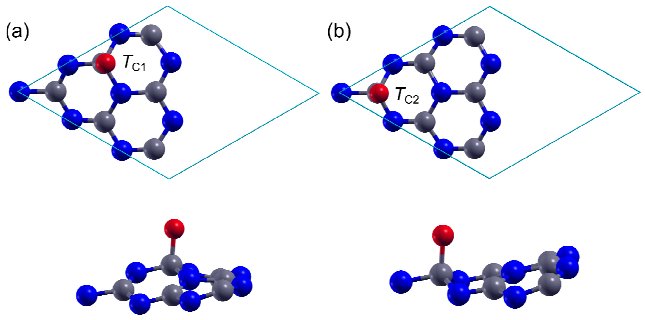

Figure 1. (color online). Two energetically favored configurations of fluorinated g-C_3N_4. Top (top panel) and side (bottom panel) views of g-C_3N_4 with one F atom absorbed at the (a) T_{C1} and (b) T_{C2} sites. Grey, blue, and red balls represent C, N, and F atoms, respectively.

Experimentally, the synthesis of fluorinated g-C_3N_4 nanosheets has been carried out employing a directly incorporating of different amount of NH_4F (x = 0, 0.5, 1.0, 2.0 g) into the classical carbon nitride condensation. For convenience, we denoted these samples as CNF-0, CNF-1.2 %, CNF-3.3% and CNF-6.5%, respectively, where x% represent the atom concentration of the fluorine in the samples obtained by X-ray photoelectron spectroscopy (XPS) measurement. X-ray diffraction analysis (XRD) shown in figure 2a reveals the graphite like packing of all products, showing the typical (002) interlayer-stacking peak around 27.4°, which is corresponding to an interlayer distance of d=0.33 nm for the fluorinated g-C_3N_4, as well-known for pure g-C_3N_4.[34] The (002) peak becomes broader and gradually less intense with increasing the concentration of fluorine, which indicates disturbance of graphitic structure, potentially by the fluorine functionality. Figure 2b is the transmission electron microscopy (TEM) image of the product, showing free-standing nanosheets feature. Also, the nearly transparent feature of the nanosheets indicates its ultrathin thickness. The well-defined Tyndall effect of the fluorinated g-C_3N_4 nanosheet solution as displayed in the inset of figure 2b indicates the presence of highly monodisperse ultrathin nanosheets in water. Besides, the thickness of the as-obtained sample was measured by tapping-mode Atomic force microscopy (AFM). As shown in figure 2c, the thickness is about 4 nm, indicating the successful production of ultrathin nanosheets. Figure 2d shows the typical TEM bright field image of few-layer fluorinated g-C_3N_4 nanosheets and the represent mapping of F, C and N from the region, which suggest homogeneous distribution of constituents across the nanosheets.

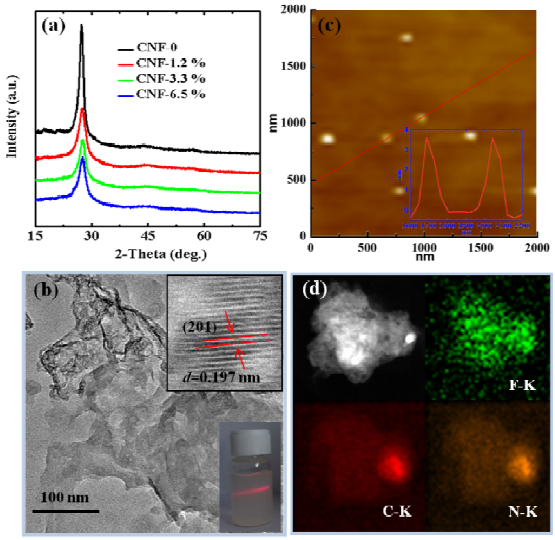

Figure 2. (color online) (a) XRD patterns for fluorinated g-C_3N_4 nanosheets CNF-x. (b) AFM image and the corresponding height profile for the fluorinated g-C_3N_4 nanosheets. (c) TEM, HRTEM and the corresponding colloidal water dispersion displaying the Tyndall effect. (d) The elemental mapping for the fluorination- g-C_3N_4 nanosheets.

Owing to the electronegativity of fluorine and nitrogen,

calculation results indicate that the doped fluorine is certainly not bound to the nitrogen, but to the carbon, resulting in a partial conversion of C-sp^2 to C-sp^3, which may lead to lower in plane order of the material.[35] Both XPS and Fourier transform infrared spectrometer (FTIR) results for the fluorinated g-C_3N_4 nanosheets also confirmed this. As shown in figure 3a, the high resolution XPS spectrum of N 1s could be fitted into four kinds of binding energy (sample CNF-3.3 %). The main N 1s peak at 398.6 eV corresponds to sp^2 hybridized aromatic N bonded to carbon atoms (C=N–C); the peak at 399.5 eV is assigned to the tertiary N bonded to carbon atoms in the form of N–$(C)_3$ or H–N–$(C)_2$; the weaker peak with high binding energy at 400.8 eV is attributed to quaternary N bonded three carbon atoms in the aromatic cycles and 404.2 eV to the pi-excitations, which agree with previously reports of g-C_3N_4.[36,37] However, for the C 1s peak shown in figure 3b, besides the common three peaks at binding energies of 284.6, 286.3 and 288.2 eV for the primitive g-C_3N_4, a new peak appears, which is caused by the F introduction and can be signed as C-F coordination.[38] In addition, The F 1s XPS peak at 686.2 eV shown in figure 3c can be assigned to the fluorine attached to carbon as previous reports.[39] In the FTIR spectra shown in figure 3d, the fluorinated materials exhibit a new band at 1220 cm^{-1} compared with the unmodified parental g-C_3N_4, which can be attributed to the stretching mode of C-F bond.[40] FTIR results also features the typical C-N heterocycle stretches in the 1200-1600 cm^{-1} and the breathing mode of the tris-triazine units at 800 cm^{-1}, as the unmodified g-C_3N_4, which supports the formation of extended network of C-N-C bonds. Above results indicate we have synthesized ultrathin metal-free fluorinated g-C_3N_4 nanosheets successfully.

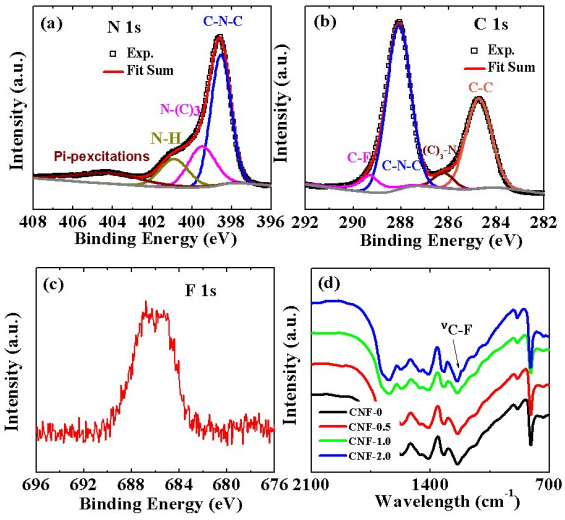

Figure 3. (color online) The high resolution XPS spectrum for sample CNF-3.3%. (a) N 1s (b) C 1s, and (c) F 1s. (d) FTIR spectrum for g-C_3N_4 nanosheets with different fluorine contents.

Static magnetization had been fruitfully exploited to probe the magnetic response of fluorinated g-C_3N_4 nanosheets. Since the orientation of the nanosheets in our samples was random, the detected magnetization signals of the samples were an average of fluorinated g-C_3N_4 nanosheets over all possible orientations. And we didn't observe any difference in the response for different orientations of applied magnetic field. Pristine un-fluorinated g-C_3N_4 nanosheets were nearly diamagnetic with a susceptibility of -8.3×10−8 emu/g•Oe (Figure S2†). However, with F absorbed, the C-N-F system developed distinct ferromagnetic signal. Figure 4a shows the Zero-field-cooled (ZFC) and field-cooled (FC) temperature dependent magnetization curves of the sample CNF-3.3% in the temperature ranging from 5 to 300 K. Obviously, ZFC and FC curves showed distinct difference in the temperature range, revealing Curie temperature is higher than 300 K. Most importantly, there is no block temperature appearance in ZFC curve, which clearly reveals that there are no ferromagnetic clusters in our sample and provides evidence for ferromagnetism in the samples. The ferromagnetic behavior was also confirmed by isothermal magnetization versus applied magnetic field (*M-H*) measurements from 10 to 700 K, where the magnetization values were obtained after subtraction of a linear background contribution (shown in Figure 4b). Ferromagnetic hysteresis from the sample CNF-3.3 % was apparent, with saturation magnetization of 0.011 emu/g and coercivity of 145 Oe at 300 K, which is comparable to the reported behavior of other metal-free nanosheets.[41] Electron spin resonance (ESR) results give further evidence for the ferromagnetism of the samples (shown in Figure S3†). As can be seen in Figure 4b, the saturation magnetization values differed by less than 50 % between 300 K and 700 K, indicating that the Curie temperature (T_C) of the CNF-3.3% nanosheets is higher than 700 K. By using the superconducting quantum interferometer device (SQUID) magnetometer from Quantum Design and vibrating sample magnetometer (VSM) equipped with a high temperature chamber, we could get the information of M_s dependence on temperature for the sample CNF-3.3%. As shown in figure 4c, the date can be well fitted by the equation of $M(T)=A(1-T/T_C)^{\beta}$, which is common for a ferromagnetic material.[42] In the equation, A is a coefficient related to the spontaneous magnetization, T_C is the ferromagnetic Curie temperature, and β is the critical exponent. The best fitting curve ($T<T_C$) is shown by red curve, where the fitted sample's Cure temperature is about 733 K. Such high T_C ferromagnetism in fluorinated g-C_3N_4 nanosheets makes them promising candidates for application in spintronic devices. Besides, we also studied the affection of amount of fluoride on the magnetic properties of the g-C_3N_4 nanosheets. As can be seen from figure 4d, the g-C_3N_4 nanosheets with different F concentrations show different saturation magnetization values, indicating that the ferromagnetism of the samples can be tuned by changing the concentration of the adsorption F atoms.

In addition to the magnetic response described, two other magnetic features imposed on the ferromagnetic signals of the fluorinated g-C_3N_4 nanosheets had been observed. One is a small but finite paramagnetic upturn as the temperature decreased to 15 K (Figure S4†). A paramagnetic upturn at low temperature was also exhibited in C-based materials. Sepioni *et al.* suggested that this behavior in graphene was related to a small number of unpassivated or unreconstructed point defects

and zigzag edges.[43,44] As pointed out in our previous report, point defects may affect the magnetic properties of g-C_3N_4 nanosheets,[21] thus the contribution of defects to ferromagnetism observed in fluorinated g-C_3N_4 nanosheets should be carefully taken into account. The carbon and nitrogen stoichiometry determined by elemental analysis (Table S1) shows that the products are very close to the ideal value of C_3N_4 (theoretical C/N is 0.75), indicating that little defects sites existence in the samples. What's more, results indicate that the unmodified g-C_3N_4 nanosheets show very weak ferromagnetism after deducted the diamagnetic signal. Because all the samples were fabricated by only changing the amount of NH_4F with other parameters identical, the contribution of defects to ferromagnetism observed in fluorinated g-C_3N_4 nanosheets could be neglect. Furthermore, inductively coupled plasma atomic emission spectrometer (ICP) results indicate that the measured content of magnetic metal impurities in CNF-3.3 % nanosheets was below 10 ppm (Table S2), which was not sufficient to produce the ferromagnetic signal.[45] These results indicate that the observed ferromagnetism of sample CNF-x mainly attributes to the topologically fluorinated. Recently, effect of adsorption atoms, such as H, F, *et al*, on electromagnetic property in otherwise 2D nanosheets such as BN and Silicene were also reported,[46-48] where the magnetic properties above room temperature were predicted or experimentally performed. These reports materials are comparable to fluorinated g-C_3N_4 in our case, which are quite promising for their potential applications in spintronics.

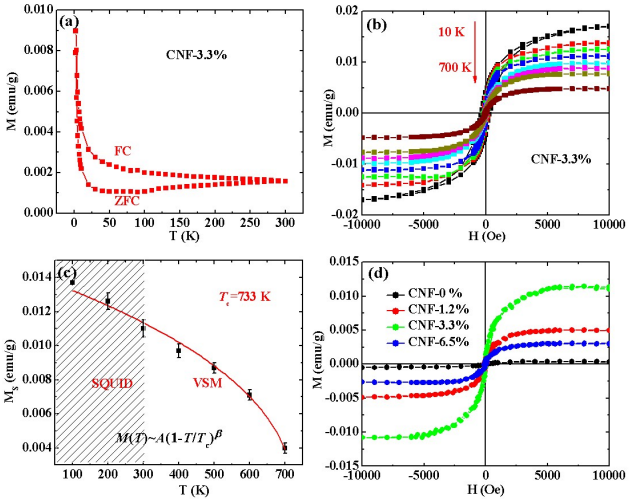

Figure 4. (color online) (a) ZFC and FC curves of CNF-3.3% under a measuring field of 200 Oe. (b) Magnetization loops for sample CNF-3.3% at different temperature (from 10~700 K), where the magnetization values were obtained after subtraction of a linear background contribution. (c) M_s dependence on temperature for sample CNF-3.3%, by fitting which the Curie temperature (T_c) of the sample is anticipated to be 733 K. (d) Magnetization loops for g-C_3N_4 nanosheets with different fluorine contents, where the magnetization values were obtained after subtraction of a linear background contribution.

To understand the above observed ferromagnetism in experiment, we resort to the spin-polarized first-principles calculations. The spin density distribution of monolayer g-C_3N_4 with one fluorine atom absorbed at the T_{C1} site is displayed in figure 5a. Our findings are very insightful. (i) One absorbed fluorine atom did induce a magnetic moment of 1.0 μB per unit cell. (ii) These local magnetic moment mainly locate on the N atoms, demonstrating a *p*-orbital (dumbbell-like) feature. (iii) The induced magnetic moment increases with the distance between the N and F atoms. More interestingly, this fluorinated g-C_3N_4 still remains a semiconducting character in the spin-up polarization, as shown in figure 5b. By contrast, one band crosses the Fermi energy level with spin-down polarization, appearing a metallic feature, as shown in figure 5d. This means fluorinated g-C_3N_4 is a half-metal with 100% spin polarization, which is very promising for future device applications in spintronics. The spin-resolved total DOS is given in figure 5c. It clearly shows that an obvious spin split appears near the Fermi energy level, being consistent with those spin-polarized band structures. Actually, the mechanism of F-adsorption-induced ferromagnetism here is quite similar to that proposed in the carbon-doped g-C_3N_4, i.e., F draws electrons from g-C_3N_4, leading to hole-doping.[22] The charge redistribution around the N atoms results in electron spin-polarization, where these overlapped magnetic moments induce intrinsic ferromagnetism in g-C_3N_4 ultrathin nanosheets.

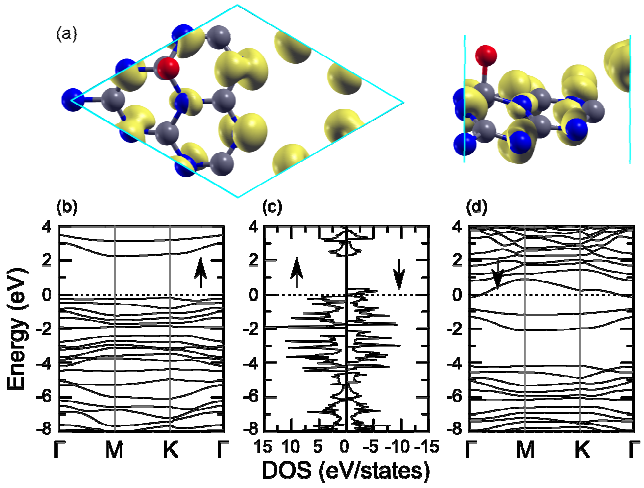

Figure 5. (color online). (a) Top (left panel) and side (right panel) views of spin density distributions of single g-C_3N_4 layer with one F atom absorbed at the T_{C1} site. The isovalue is set to 0.02 e/Å^3. (b) Spin-up band structure. The dotted line represents the Fermi energy level. (c) Spin-resolved total DOS. (d) Spin-down band structure. The arrows denote the spin orientations.

In order to study the possible reconstruction and magnetic coupling between local magnetic moments, we adopted large-size supercells containing four primitive cells (denoted as 2×2). Starting from different initial spin arrangements, self-consistent calculations lead to two types of magnetic orderings. One has the local magnetic moments aligned in a ferromagnetic way (FM), similar to the results of the primitive cells. The other one has the local magnetic moments aligned in an "antiferromagnetic" way (AFM).[49] Our calculations showed that the FM state of fluorinated g-C_3N_4

single layer is energetically more stable than the AFM state about 160 meV per supercell. This implies that the local magnetic moments favor FM ordering at zero temperature with a total magnetic moment of 4.0 μ_B in the 2×2 supercell. To sum up, above calculations results indicate that the spin moments induced by fluorine adsorption on g-C_3N_4 nanosheets can be ferromagnetically coupled to exhibit long rang magnetic ordering, which is corresponding to the experimental results.

Conclusions

To conclude, we provide the experimental and theoretical evidence that the high temperature ferromagnetism could be achieved in ultrathin metal-free materials of g-C_3N_4 by topological fluorine adsorption. Careful control experiments confirmed that the observed magnetic order originates from the fluorine adsorption rather than from possible contamination of extrinsic magnetic impurities. This work broadens our horizon for achieving magnetic couple modulation in metal-free materials. Meanwhile, we anticipate that fluorination will provide new intriguing strategy to regulate the electronic structure of materials, endowing a new opportunity to induce spin related information in other 2D metal-free ultrathin nanosheets.

Acknowledgements

This work is supported by National Basic Research Program of China (Grant No. 2012CB933101), the National Natural Science Fundation of China (Grant No. 51371093, 51202101, 11474137, 11274146 and 11034004), Program for Changjiang Scholars and Innovative Research Team in University (Grant No. IRT1251) and the Specialized Research Fund for the Doctoral Program of Higher Education (20120211120005).

METHODS

Preparation of ultrathin fluorinated g-C_3N_4 nanosheets: In a typical synthetic procedure, 3 g dicyanamide and different amount of NH_4F (x = 0, 0.5, 1.0, 2.0 g) were added into the aqueous solution and the mixture was heated in an oil bath at 60 ℃ until removal of water and formation of a white solid. The white solid was then transferred into a crucible and heated over 4 h to reach a temperature of 550 ℃ and tempered at this temperature for 2 h. This was followed by cooling the sample naturally to room temperature. Finally, the obtained fluorinated g-C_3N_4 powder were dispersed in water and then ultrasound for about 10 hours. The initial formed suspension was then centrifuged at about 5000 rmp to remove the residual un-exfoliated nanoparticles.

Caution: HF is highly corrosive and toxic. Care should be taken to ensure that the oven is putted in the cabinet and never blocked, and the exhausting gas should be fed through NaOH solution bath cooling traps system to collect the remnant toxic gas.

Characterization: X-ray diffraction (XRD, X' Pert PRO PHILIPS with Cu Kα radiation) was employed to study the crystal structure. The morphology of the samples were obtained by using the scanning electron microscope (SEM, Hitachi S-4800) and high resolution transmission electron microscopy (HRTEM, TecnaiTM G2 F30, FEI, USA). Atomic force microscopy (AFM) study in the present work was performed by means of Veeco DI Nanoscope Multi Mode V system. X-ray photoelectron spectroscopy (XPS, VG ESCALAB 210) was utilized to determine the bonding characteristics of the samples. The composition was confirmed by an inductively coupled plasma atomic emission spectrometer (ICP, ER/S). The element analyzer (Varoi EL) was employed to study the C/N rations of the samples. The infrared absorption spectra of the samples were conducted with the KBr pellet method on a Fourier transform infrared spectrometer (FTIR; NEXUS 670, Thermo Nicolet Corp., Madison, WI, USA) in the range of 500 to 3500 cm−1. The measurements of magnetic properties were made using the Quantum Design MPMS magnetometer based on superconducting quantum interference device (SQUID) and vibrating sample magnetometer equipped with a high temperature chamber (VSM, VSM Model EV9, MicroSense, LLC). Electron spin resonance (ESR JEOL, JES-FA300, microwave frequency is 8.984 GHz) measurement was employed to study the resonance field of the samples.

Calculations details: The electronic properties are performed via VASP code, which is based on density functional theory with the generalized gradient approximation (GGA) of Perdew-Burke-Ernzerhof (PBE) for the exchange-correlation (XC) potential within the projector augmented wave method. The cutoff energy for plane waves is set to be 400 eV, and the vacuum space is at least 15 Å, which is large enough to avoid the interaction between periodic images. A 9×9×1 Monkhorst-Pack grid is used for the sampling of the Brillouin zone during geometry optimization and a higher 15×15×1 Monkhorst-Pack grid for self-consistent calculations. All the atoms in the unit cell were allowed to relax, and the convergence of force is set to 0.01 eV/ Å. The model of 2×2 supercell with one carbon atom removed was used to simulate the electronic and magnetic properties.

Notes and references

*Key Laboratory for Magnetism and Magnetic Materials of MOE, Key Laboratory of Special Function Materials and Structure Design, Ministry of Education, Lanzhou University, Lanzhou 730000, P. R. China. Fax: +86 0931 8914160; Tel: +86 0931 8914160; *E-mail: sims@lzu.edu.cn;xueds@lzu.edu.cn.*

† Electronic Supplementary Information (ESI) available]. Detailed description for the experimental and theoretical method based on the ferromagnetism of the fluorinated metal-free materials of g-C_3N_4 nanosheets. As well as, the XPS results for sample CNF-0, FTIR and ESR results for sample CNF-x, primitive M-H curves for sample CNF-3.3%, and the C/N rations and ICP results for sample CNF-x. See DOI: 10.1039/b000000x/

1 S. A. Wolf, D. D. Awschalom, R. A. Buhrman, J. M. Daughton, S. von Molnar, M. L. Roukes, A. Y. Chtchelkanova, D. M. Treger, Science, 294, 1488 (2001).

2 Y. Ohno, D. K. Young, B. Beschoten, F. Matsukura, H. Ohno, D. D. Awschalom, Nature, 402, 790 (1999).

3 D. Gao, G. Yang, J. Li, J. Zhang, D. S. Xue, J. Phys. Chem. C 114, 18347 (2010).
4 J. M. D.Coey, Solid State Sci., 7, 660 (2005).
5 T. Y. Yang, J. Balakrishnan, F. Volmer, A. Avsar, M. Jaiswal, J. Samm, S. R. Ali, A. Pachoud, M. Zeng, M. Popinciuc, et al. Phys. Rev. Lett. 107, 047206 (2011).
6 A. Hashmi, J. Hong, Sci. Rep. 4, 4374 (2014).
7 Z. Zhang, X. C. Zeng, W. Guo, J. Am. Chem. Soc. 133, 14831 (2011).
8 J. Zeng, K. Chen, C. Sun, Phys. Chem. Chem. Phys. 14, 8032 (2012).
9 M. A. H. Vozmediano, M. P. López-Sancho, T. Stauber, F. Guinea, Phys. Rev. B, 72, 155121 (2005).
10 X. Hong, K. Zou, B. Wang, S. H. Cheng, J. Zhu, Phys. Rev. Lett. 108, 226602 (2012).
11 F. Withers, M. Dubois, A. K. Savchenko, Phys. Rev. B 82, 073403 (2010).
12 M. Groenewolt, M. Antonietti, Adv. Mater., 17, 1789 (2005).
13 S. C.Yan, Z. S. Li, Z. G. Zou, Langmuir, 25, 10397 (2009).
14 X.Wang, K. Maeda, A. Thomas, K. Takanabe, G. Xin, J. M. Carlsson, K. Domen, M. Antonietti, Nat. Mater., 8, 76 (2009).
15 X. H. Li, X. Wang, M. Antonietti, Chem. Sci., 3, 2170 (2012).
16 J. Zhang, M. Grzelczak, Y. Hou, K. Maeda, K. Domen, X. Fu, M. Antonietti, X. Wang, Chem. Sci., 3, 443 (2012).
17 G. Liu, P. Niu, C. Sun, S. C. Smith, Z. Chen, G. Q. Lu, H. M. Cheng, J. Am. Chem. Soc., 132, 11642 (2010).
18 Y. Wang, J. Zhang, X. Wang, M. Antonietti, H. Li, Angew. Chem. Int. Ed., 49, 3356 (2010).
19 M. P. López-Sancho, F. De Juan, M. A. H. Vozmediano, Phys. Rev. B 79, 075413 (2009).
20 M. S.Si, D. S. Xue, Phys. Rev. B 75, 193409 (2007).
21 D. Q. Gao, Q. Xu, J. Zhang, Z. L. Yang, M. S. Si, Z. J. Yan, D. S. Xue, Nanoscale 6, 2577 (2014).
22 X. M. Zhang, M. W. Zhao, A. Z. Wang, X. P. Wang, A. Du, J. Mater. Chem. C 1, 6265 (2013).
23 Y. Xu, S. P. Gao, 37, 11072 (2012).
24 X. Li, J. Zhou, Q. Wang, Y. Kawazoe, P. Jena, J. Phys. Chem. Lett. 4, 259 (2013).
25 X. Li, Q. Wang, Phys. Chem. Chem. Phys., 14, 2065 (2012).
26 A. Du, S. Sanvito, S. C. Smith, Phys.Rev.Lett. 108, 197207 (2012).
27 H. Y. Liu, Z. F. Hou, C. H. Hu, Y. Yang, Z. Z. Zhu, J. Phys. Chem. C 116, 18193 (2012).
28 Z. H. Zhang, W. L. Guo, J. Am. Chem. Soc. 131, 6874 (2009).
29 J. T. Robinson, J. S. Burgess, C. E. Junkermeier, S. C. Badescu, T. L. Reinecke, F. K. Perkins, M. K. Zalalutdniov, J. W. Baldwin, J. C. Culbertson, P. E. Sheehan, et al. Nano Lett. 10, 3001 (2010).
30 R. R. Nair, W. Ren, R. Jalil, I. Riaz, V. G. Kravets, L. Britnell, P. Blake, F. Schedin, A. S. Mayorov, S. J. Yuan, M. I. Katsnelson, H. M. Cheng, W. Strupinski, L. G. Bulusheva, A. V. Okotrub, I. V. Grigorieva, A. N. Grigorenko, K. S. Novoselov, A. K. Geim, Small, 6, 2877 (2010).
31 J. T. Robinson, J. S. Burgess, C. E. Junkermeier, S. C. Badescu, T. L. Reinecke, F. K. Perkins, M. K. Zalalutdniov, J. W. Baldwin, J. C. Culbertson, P. E. Sheehan, E. S. Snow, Nano Lett., 10, 3001 (2010).
32 Y. D. Ma, Y. Dai, M. Guo, C. W. Niu, L.Yu, B. B. Huang, Nanoscale, 3, 2301 (2011).
33 Y. Wang, Y. Di, M. Antonietti, H. R. Li, X. F. Chen, X. C. Wang, Chem. Mater. 22, 5119 (2010).
34 F. Dong, L. Wu, Y. Sun, M. Fu, Z. Wu, S. C. Lee, J. Mater. Chem. 21, 15171 (2011).
35 H. Wang, X. D. Zhang, J. F. Xie, J. J. Zhang, P. Ma, B. C. Pan, Yi Xie, Nanoscale, 7, 5152 (2015).
36 L. Yang, P. W. May, L. Yin, T. B. Scott, J. A. Smith, K. N. Rosser, Nanotechnology 17, 5798 (2006).
37 C. L. Schmidt, M. Jansen, J. Mater. Chem. 20, 4183 (2010).
38 M. L. Shofner, V. N. Khabashesku, E. V. Barrera, Chem. Mater. 18, 906 (2006).
39 I. Palchan, M. Crespin, H. Estradeszwarckopf, B. Rousseau. Chem. Phys. Lett. 157, 321 (1989).
40 A. Hamwi, M. Daoud, J. C. Cousseins, Synth. Met. 26, 89 (1988).
41 K. Xu, X. L. Li, P.Z. Chen, D. Zhou, C. Z. Wu, Y. Q. Guo, L. D. Zhang, J. Y. Zhao, X. J. Wu, Y. Xie, Chem. Sci. 6, 283 (2015).
42 H. E. Stanley, Oxford University Press, Oxford, 1987.
43 M. Sepioni, R. R. Nair, S. Rablen, J. Narayanan, F. Tuna, R. Winpenny, A. K. Geim, I. V. Grigorieva, Phys. Rev. Lett. 105, 207205 (2010) .
44 X. L. Ding, H. Sun, X. M. Xie, H. C. Ren, F. Q. Huang, M. H. Jiang, Phys. Rev. B 84, 174417 (2011).
45 D. Q. Gao, S. P. Shi, K. Tao, B. R. Xia, D. S. Xue, Nanoscale, 7, 4211 (2015).
46 M. Du, X. L. Li, A. Z. Wang, Y. Z. Wu, X. P. Hao, M. W. Zhao, Angew. Chem. Int. Ed. 53, 3645 (2014).
47 C. W.Zhang, S. S. Yan, J. Phys. Chem. C, 116 (6), 4163 (2012).
48 R. W. Zhang, C. W. Zhang, W. X. Ji, S. J. Hu, S. S. Yan, S. S. Li, P. Li, P. J. Wang, Y. S. Liu, J. Phys. Chem. C, 118, 25278 (2014).
49 C. Zhao, Z. Xu, H. Wang, J. K. Wei, W. L. Wang, X. D. Bai, E. G. Wang, Adv. Funct. Mater. 38, 5985 (2014).